JOURNAL OF THERMOPHYSICS AND HEAT TRANSFER
Vol. 21, No. 3, July–September 2007

Turbulent Navier–Stokes Simulations of Heat Transfer with Complex Wall Temperature Variations

Eric C. Marineau* and Joseph A. Schetz†
Virginia Polytechnic Institute and State University, Blacksburg, Virginia 24061
and
Reece E. Neel‡
AeroSoft, Inc., Blacksburg, Virginia 24061

DOI: 10.2514/1.26007

Numerical simulations focusing on convective heat transfer with complex wall temperature variations, as well as conjugate heat transfer problems involving solids are performed. Simulations are made using the commercial computational fluid dynamics code, which solves the Reynolds-averaged Navier–Stokes equations. This computational fluid dynamics code has been modified by adding a solid heat conduction solver, enabling the coupling of Reynolds-averaged Navier–Stokes equations with the heat equation for an isotropic solid. Validation cases involving convective heat transfer are considered using both one- and two-equation turbulence models. Predicted Stanton numbers for low Mach number turbulent boundary layers agree with experimental results for a constant wall temperature, a step, and a double pulse in wall temperature. Simulations of supersonic boundary layers with a step in wall temperature are also performed. Good agreement is found for velocity and temperature profiles when compared with measurement, as well as for the skin friction and Stanton number. The flowfield and wall temperature distribution inside a supersonic cooled nozzle is computed using a new conjugate heat transfer algorithm. Results agree well with measurements.

I. Introduction

THE coupling of heat transfer at a solid/fluid interface is known as conjugate heat transfer (CHT). CHT problems are commonly found in real-world applications such as turbomachinery, reentry vehicles, laser irradiation applications, heating ducts, and more. To properly simulate a conjugate heat transfer problem, the method should be able to accurately model the convective heat transfer in the fluid and the conductive heat transfer in the solid.

CHT capabilities have been added to GASP, allowing tight coupling of the Reynolds-averaged Navier–Stokes (RANS) equations in the fluid to the heat conduction equation in the solid. Because conjugate heat transfer problems involve convective heat transfer at the fluid–solid interface, accurate modeling of convection is critical when solving these problems. Therefore, several cases involving convective heat transfer for low and high Mach number boundary layers are presented. These cases serve as validation problems for the fluid flow solver.

Three low Mach number cases are considered, namely, a heated wall at constant temperature, a step in wall temperature, and a double heat pulse. Numerical results of the Stanton number are compared with experimental results from Reynolds et al. [1,2].

Three supersonic cases are considered, which include an adiabatic wall case and a step in the wall temperature with ratio of wall to recovery temperature, T_w/T_r, of 1.5 and 2, respectively. Skin friction, Stanton number, and velocity and temperature profiles are compared with experimental results from Debieve et al. [3]. A single conjugate heat transfer problem is considered, namely, an axisymmetric nozzle with an exit Mach number of 2.6 involving heated flow of air and a water-cooled wall. The flowfield and the wall temperature distribution are computed and compared with measurements from Back et al. [4].

Presented as Paper 3087 at the Joint AIAA/ASME Thermophysics and Heat Transfer, San Francisco, CA, 5–8 June 2006; received 19 June 2006; revision received 20 December 2006; accepted for publication 21 December 2006.

*Graduate Research Assistant, Department of Aerospace and Ocean Engineering, 215 Randolph Hall, Blacksburg, VA 24061. Student Member AIAA.

†Holder of the Fred D. Durham Chair, Department of Aerospace and Ocean Engineering, 215 Randolph Hall, Blacksburg, VA 24061. Fellow AIAA.

‡Research Scientist, AeroSoft, Inc., Blacksburg, VA 24061. Member AIAA.

II. Flow Solver

A recent version of GASP, version 4.3, was used for this study. This is a commercial computational fluid dynamics (CFD) flow solver developed by AeroSoft, Inc. [5]. It solves the integral form of the time-dependent RANS equations in three dimensions.

To model turbulence, the code has an array of options. These include the Baldwin–Lomax [6] algebraic model in any two logical directions, the one-equation Spalart–Allmaras [7] model, two-equation models based upon the k–ω and k–ϵ equations, and a second-order Reynolds stress closure model by Wilcox denoted as the stress-ω model [8]. The k–ω models include Wilcox's 1988 [9] and 1998 [8] high Reynolds number models, Wilcox's 1998 low Reynolds number model [8], and Menter's shear stress transport (SST) model [10]. For the k–ϵ models, the code supports a high Reynolds number model [11], Chien's model [12], and the model by Lam and Bremhorst [13]. All of the preceding models support user-input, intermittency values for transition modeling. Additional information and validation of the turbulence modeling can be found in Neel et al. [14]. All single and multi-equation models can be run uncoupled from the primary flow equations for more efficient CPU times.

The turbulent heat fluxes are modeled using the turbulent Prandtl number Pr_t, which is assumed to be constant across the boundary layer. The turbulent heat fluxes are expressed in the following way:

$$-\widetilde{u_i''T''} = \alpha_t \frac{\partial \tilde{T}}{\partial x_i} = \frac{\nu_t}{Pr_t}\frac{\partial \tilde{T}}{\partial x_i} \tag{1}$$

where α_t is the turbulent thermal diffusivity, ν_t is the dynamic eddy viscosity and $\tilde{(\ )}$ denotes Favre averaging, and $(\ )''$ the fluctuation of $(\ )$, respectively. In this formulation, a similarity between turbulent heat and momentum transfer is assumed because the turbulent thermal diffusivity is directly computed from the dynamic eddy

viscosity [15]. For wall-bounded flow, experimental evidence shows that Pr_t increases close to the wall. However when the Prandtl number is less than one, the value of Pr_t at $y^+ < 7$ or 8 has negligible effect on calculations [16]. Therefore, for air, the constant Prandtl number approximation is reasonable. Kays et al. [16] presents a correlation for the variation of Pr_t across a boundary layer without pressure gradients which agrees reasonably well with experimental data.

Another approach involves modeling the temperature fluctuations [15,17–19]. Complexity and computational cost are increased as two additional equations for the temperature variance and its dissipation rate need to be coupled to the turbulence model. This approach is being investigated for future work.

III. Heat Equation and Conjugate Heat Transfer Modeling

A solver for the three-dimensional heat conduction equation has been added to GASP to perform conjugate heat transfer problems. The time-dependent heat transfer equation for an isotropic, solid continuum is expressed as

$$\rho c_v \frac{\partial T}{\partial t} = \frac{\partial}{\partial x}\left(k\frac{\partial T}{\partial x}\right) + \frac{\partial}{\partial y}\left(k\frac{\partial T}{\partial y}\right) + \frac{\partial}{\partial z}\left(k\frac{\partial T}{\partial z}\right) + \dot{q} \qquad (2)$$

where ρ is the material density, c_v is the specific heat, and k is the thermal conductivity, all of which can be functions of temperature. The source term $\dot{q}$ represents an internal energy source. This equation can be recast into integral form as

$$\rho c_v \frac{\partial}{\partial t}\iiint T\,\mathrm{d}V = \oint_A (k(\nabla T \cdot \hat{\mathbf{n}})\,\mathrm{d}A + \iiint \dot{q}\,\mathrm{d}V \qquad (3)$$

which lends itself to the finite volume implementation. In the finite volume solver, the unknown (in our case temperature) is assumed to be volume averaged over each cell in the mesh. This can be expressed as,

$$\bar{T} = \frac{1}{V}\iiint T\,\mathrm{d}V \qquad (4)$$

where the bar over T indicates a volume average.

The diffusive term (heat flux) is computed in the same fashion as the viscous terms used in the Navier–Stokes solver. This yields a second-order-accurate central difference formulation for the diffusive flux. For time-accurate flows, the dual time-stepping algorithm is used. In this situation, the algorithm presented next is repeated for a set number of cycles in which the heat flux is converged for a given physical time step. The algorithm for performing CHT problems is now explained. In the following description, it may be helpful to refer to Fig. 1 for terminology. In this figure, the fluid dynamics zone (or grid) is on top and the shaded zone on bottom is the solid material zone. The boundary condition at a zonal boundary face (face common to both a fluid zone and a solid zone) is

$$T_{\mathrm{fw}} = T_{\mathrm{sw}} = T_w \qquad \text{(wall temperatures equal)}$$

and

$$q_{\mathrm{fw}} = -q_{\mathrm{sw}} \qquad \text{(heat fluxes equal and opposite)}$$

where

$$q_{\mathrm{fw}} = -k_f \left.\frac{\partial T}{\partial n}\right|_{\mathrm{fw}} \qquad q_{\mathrm{sw}} = -k_s \left.\frac{\partial T}{\partial n}\right|_{\mathrm{sw}}$$

When a surface heat source is present, the boundary condition becomes

$$q_{\mathrm{fw}} = -q_{\mathrm{sw}} - q_o$$

where q_o is an additional heat flux specified by the user. The preceding condition states the conservation of energy at the surface.

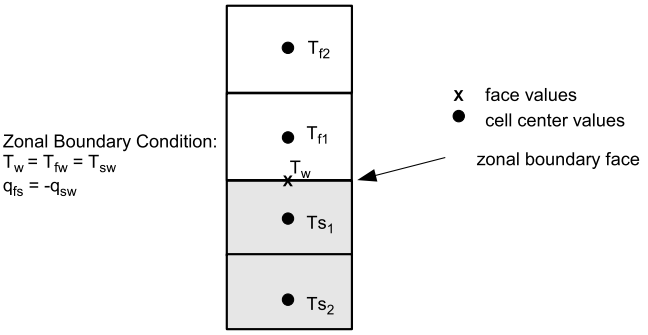

Fig. 1 Schematic of the conjugate heat transfer problem.

The algorithm covering one iteration cycle is as follows:

1) The wall temperature along the zonal boundary is computed at each boundary face. This is done by setting the heat flux for the fluid face equal to the heat flux for the solid face and solving for temperature. This results in a temperature which satisfies the constraint of an equal and opposite heat flux for each zonal boundary face. The heat flux uses a second-order, one-sided stencil for the temperature gradient at the boundary face.
2) The fluid zone is then solved. Fluxes are computed for each face and boundary conditions are applied. The unknowns (i.e., density, velocity, pressure, turbulence quantities) at each cell center are updated.
3) The wall temperature is then updated along the zonal boundary due to the updated fluid dynamic solution. Again, the condition of an equal and opposite heat flux is imposed to compute the wall temperature.
4) The solid zone temperature is then solved. Fluxes are computed for each face and boundary conditions are applied. The unknowns (temperature) at each cell center are updated.

This completes one iteration cycle. At convergence, the wall temperature for the fluid is equal to the wall temperature for the solid ($T_{\mathrm{fw}} = T_{\mathrm{sw}}$), as well as equal and opposite heat transfer fluxes.

IV. Results

The results from the validation cases will now be presented. The first set of cases pertain to a low-speed, turbulent boundary layer with arbitrary wall temperature. Three cases of increasing complexity are studied, namely, a heated wall at constant temperature, a step change in wall temperature, and a double heat pulse. Numerical results of the Stanton number are compared with experimental results from Reynolds et al. [1,2].

The second set of cases involves supersonic turbulent boundary layers. Again, there are three cases in this set which include an adiabatic wall and a step change in wall temperature with respective ratios of wall to recovery temperature, T_w/T_r, of 1.5 and 2. The final case is a supersonic cooled axisymmetric nozzle. Both the flowfield and the solid wall temperature distributions are computed using the CHT algorithm.

For both the high- and low-speed cases, the grid is clustered normal to the surface using a hyperbolic tangent distribution such that $y^+ < 1$ for the first cell from the wall. Uniform spacing is used in the x direction and the grid density is set such that the cell aspect ratio is kept under 1000. At least 40 cells were located inside the boundary layer. For each case, a grid-convergence study was performed by using mesh sequencing. Either two or three grid levels were used and created by removing every other grid point from the previous grid level. The solutions on each grid level were then compared with each other to determine if the grid level was sufficient to resolve all the relevant flow physics. In some cases, the final grid was determined by going through several cycles of the grid-convergence study. For all simulations, Roe's flux difference splitting scheme [20] was used with third-order spatial accuracy.

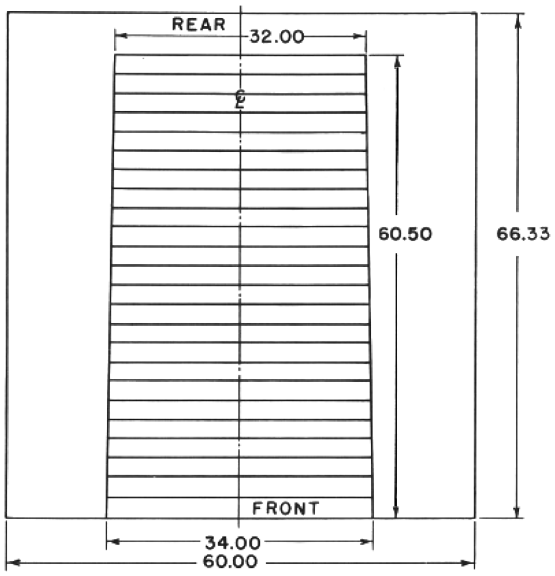

Fig. 2 Experimental apparatus; wall temperature distribution obtained with heated strips [1].

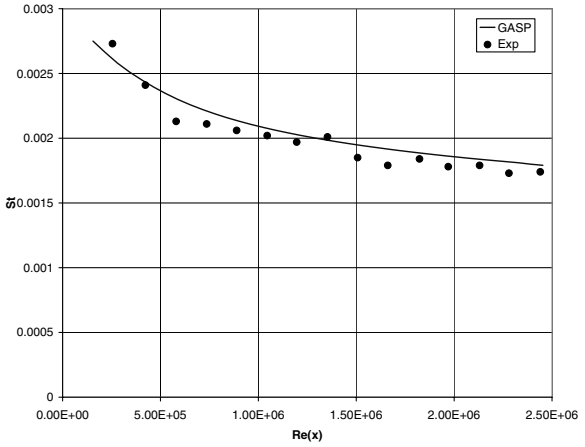

Fig. 3 Stanton number for low-velocity boundary layer on a heated wall with constant $Tw - Te = 12.8$ K compared with experiment from [1].

A. Low-Velocity Turbulent Boundary Layer with Arbitrary Wall Temperature

Three cases of low-velocity turbulent flow over a flat plate are studied. For these cases, no significant difference was found among the turbulence models used. Therefore, only the Wilcox k–ω turbulence model solutions are shown. A constant value of the turbulent Prandtl number Pr_t of 0.9 was used.

The wall temperature distribution is set by using heated strips as shown in Fig. 2. First, a heated wall at constant temperature is considered. The wall temperature is imposed as a boundary condition. Predicted Stanton numbers St are compared against experimental data from Reynolds et al. [1,2]. Both Menter's SST and Wilcox's 1998 k–ω two-equation turbulence models are used as well as the Spalart–Allmaras (S–A) one-equation turbulence model. The freestream properties are 1) $T_e = 300.7$ K, 2) $M_e = 0.111$, and 3) $\rho_e = 1.168$ kg/m^3.

The temperature of the heated wall is maintained constant at 12.8 K above the fluid freestream temperature. Results for St are depicted in Fig. 3 which generally matches experimental data.

The second low-speed case considered is a plate with an isothermal portion followed by an adiabatic region. The free stream conditions are the following: 1) $T_e = 294.7$ K, 2) $M_e = 0.089$, and 3) $\rho_e = 1.197$ kg/m^3.

Figure 4 shows both the experimental wall temperature, used as a boundary condition, and the Stanton number. As in the previous case, turbulence modeling does not significantly impact the results. It is important to note that in the experimental setup, the wall section labeled as adiabatic was not insulated; the heaters were simply turned off [2]. This explains the negative value of the Stanton number over that portion, as the flow heated over the isothermal region heats up the wall located downstream.

The next case considered is a flat plate with a double pulse in wall temperature with the following freestream conditions: 1) $T_e =$ 293.3 K, 2) $M_e = 0.108$, and 3) $\rho_e = 1.213$ kg/m^3.

The experimental wall temperature was again used to set the numerical boundary condition. These data along with the results for Stanton number are shown in Fig. 5. As for the previous case, the heaters were turned off over the section labeled adiabatic, such that the flow transfers heat to the wall in that region, which explains the negative Stanton number. Again, good agreement is seen between the numerical simulation and the experimental results.

B. Supersonic Turbulent Boundary Layer with a Step in Wall Temperature

The three cases investigated experimentally by Debieve et al. [3] are now presented. To the authors knowledge, these experimental results are the only ones for a heated turbulent boundary layer subjected to a step in wall temperature. The flow conditions and

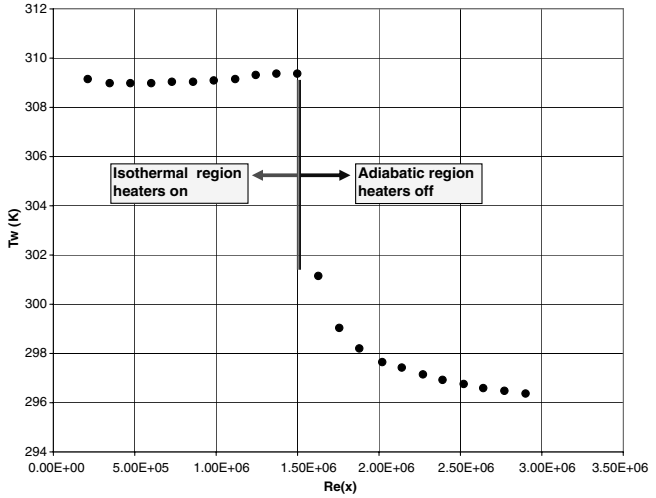

a) Wall temperature boundary condition

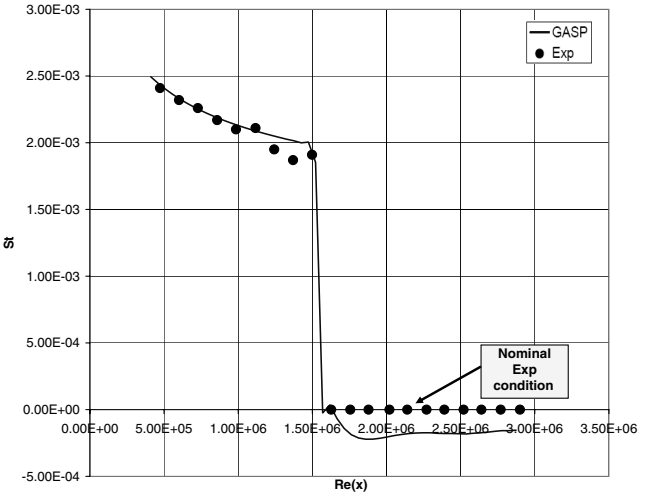

b) Stanton number for a wall temperature step

Fig. 4 Stanton number for a low-velocity boundary layer subjected to wall temperature step compared with experiment from [2].

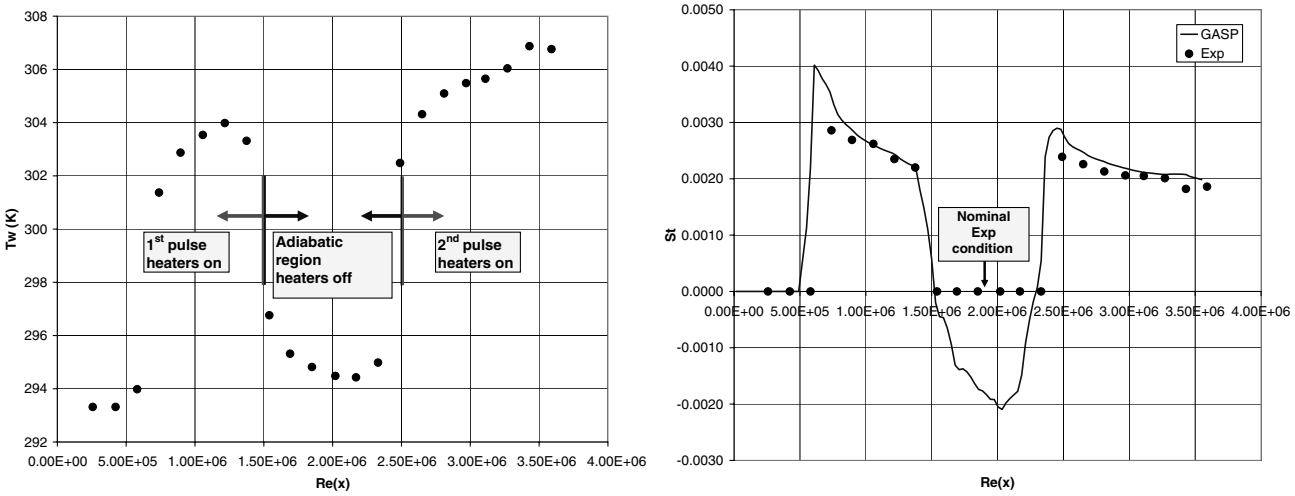

a) Wall temperature boundary condition **b) Stanton number for a double wall temperature pulse**

Fig. 5 Stanton number for a low-velocity boundary layer subjected to double pulse in wall temperature compared with experiment from [2].

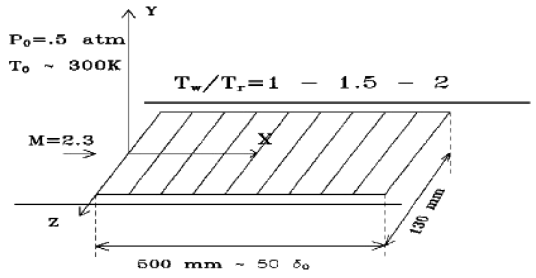

Fig. 6 Experimental configuration taken from [3].

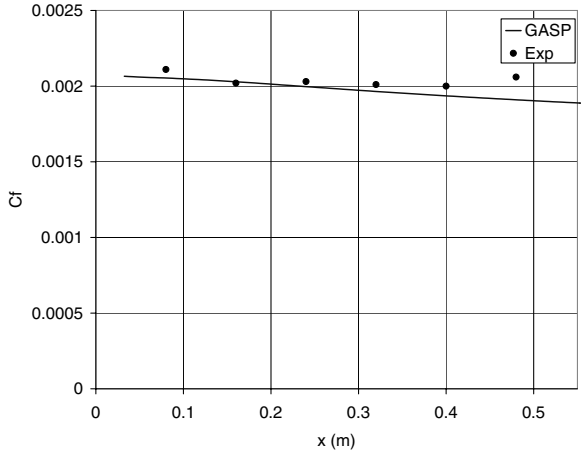

Fig. 7 Skin friction coefficient for a supersonic boundary layer with an adiabatic wall compared with results from [3].

initial boundary-layer parameters are 1) $T_0 = 300 \pm 5$ K, 2)$p_0 = 0.5 \times 10^5$ Pa $\pm$ 3%, 3) $M_e = 2.3$, 4) $\delta_0 = 10.2$ mm, and $Re_\theta = 4200$.

The experimental configuration is depicted in Fig. 6. Total temperature and velocity profiles were measured using hot-wire anemometry. The method developed in the appendix was used to generate the missing variables at the domain inlet.

The first case considered is an adiabatic wall. Good agreement is found for the skin friction, as seen in Fig. 7. Computed velocity profiles are compared with experimental results in Fig. 8. At a downstream location of 8 cm, good agreement is found close to the wall. The discrepancy away from the wall is probably due to the effect of pressure gradients in the nozzle. Because the relaxation rate varies proportionally to the inverse of $(\partial u/\partial y)$, the flow adjusts more quickly close to the wall [3] explaining the better agreement in the near-wall region. At 46 cm, the agreement is better throughout the boundary layer because the flow has more time and distance to relax. Overall, better agreement is found when using the experimental velocity profile as a boundary condition as opposed to a flat plate profile. The Menter SST turbulence model gives better agreement than Wilcox's k–ω. The Menter SST model and the boundary condition based on the experimental velocity profile are used for the two subsequent cases.

For the next two cases, a step change in wall temperature is applied at $x = 0$ with respective ratios in wall temperature to recovery temperature, T_w/T_r, equal to 1.5. and 2. Turbulent Prandtl numbers of 0.9 and 0.86 are used. It is observed that such a change does not significantly modify the velocity and temperature profile. However, a change in the turbulent Prandtl number introduces a variation in the Stanton number. Good agreement is found for the skin friction coefficient and Stanton number for both cases, as shown in Figs. 9 and 10 in which the computed values are compared with those of Debieve et al. [3]. The variation in Pr_t shifts the St curve. The two turbulent Prandtl number solutions bracket the experimental data.

Velocity and temperature profiles are shown in Figs. 11 and 12. We notice that for both T_w/T_r ratios, the agreement in velocity is better at 8 cm. Agreement in temperature is good at both stations for both T_w/T_r ratios. Temperature profiles at both stations closely match experimental results.

C. Conjugate Heat Transfer in a Cooled Nozzle

Supersonic flow inside a cooled axisymmetric convergent divergent nozzle is investigated next. The analysis is based on the experimental data reported by Back et al. [4]. Before expansion in the nozzle, the air is heated by the combustion of methanol and directed through a calming section followed by a cooled approach section of 18 in. The mass fraction of the methanol being small (compared to air), the real gas mixture can be approximated as a perfect gas. The nozzle and the approach section are water cooled on the outside of the wind-tunnel wall. The temperature distribution inside is experimentally obtained by using three thermocouples embedded at 22 locations along the nozzle wall (the first on the flow side, the second at the wall center, and the third on the cooled side). The uncertainty on the temperature measurements is approximately 2% [4]. The temperature distribution inside the wall is depicted in Fig. 13 by Back et al. [4] reported by DeLise and Naraghi [21]. The following flow conditions prevail: 1) $T_0 = 843.33$ K, and 2) $p_0 = 5.171 \times 10^5$ Pa.

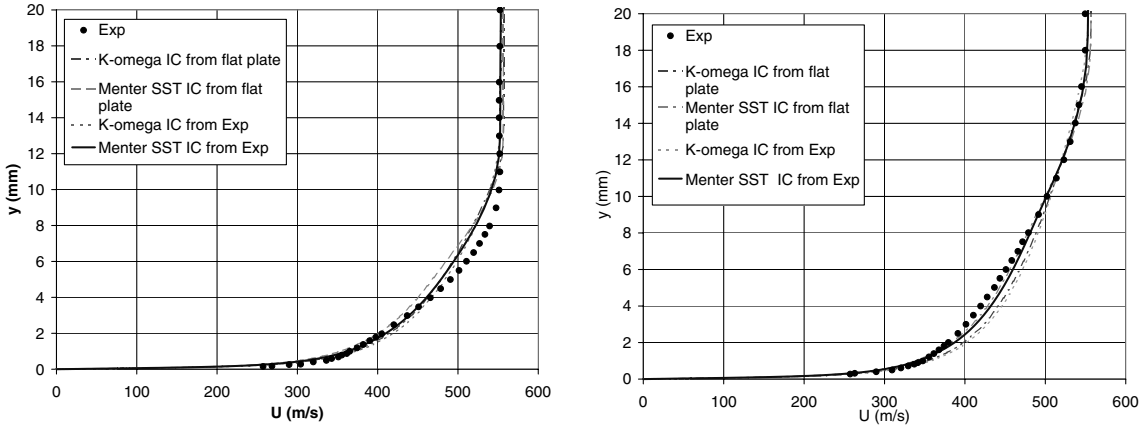

a) Velocity at 8 cm **b) Velocity at 46 cm**

Fig. 8 Velocity profiles for a supersonic boundary layer on an adiabatic wall compared with experiment from [3].

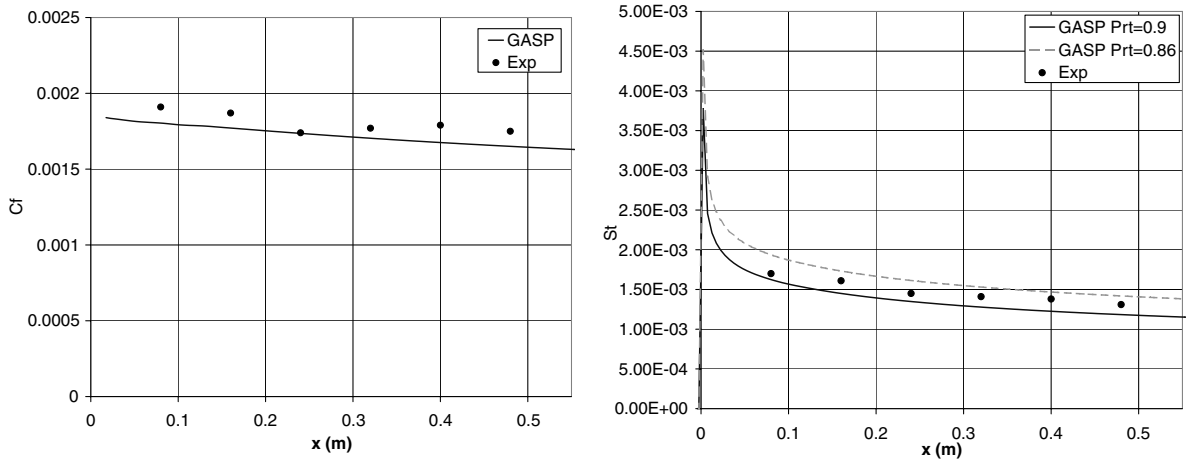

a) Skin friction **b) Stanton number for Pr_t equal to 0.9 and 0.86**

Fig. 9 Skin friction coefficient and Stanton number for supersonic boundary layer with step in wall temperature with $T_w/T_r = 1.5$ compared with results from [3].

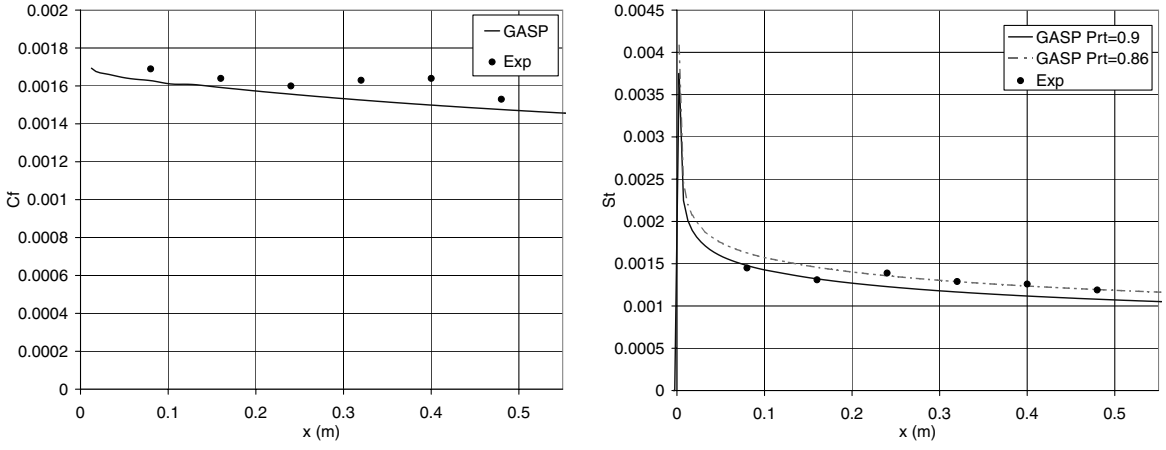

a) Skin friction **b) Stanton number for Pr_t equal to 0.9 and 0.86**

Fig. 10 Skin friction coefficient and Stanton number for supersonic boundary layer with step in wall temperature with $T_w/T_r = 2$ compared with results from [3].

This case has previously been analyzed by DeLise and Naraghi [21] and Liu et al. [22]. DeLise and Naraghi [21] did not model the heat transfer inside the solid by directly using the wall temperature on the flow side as a boundary condition. Their analysis is useful, as their results show that an algebraic turbulence model cannot be used to accurately model heat transfer in the vicinity of the throat because the favorable pressure gradient causes a reduction in turbulence intensity which in turn causes a reduction of heat transfer. This phenomenon

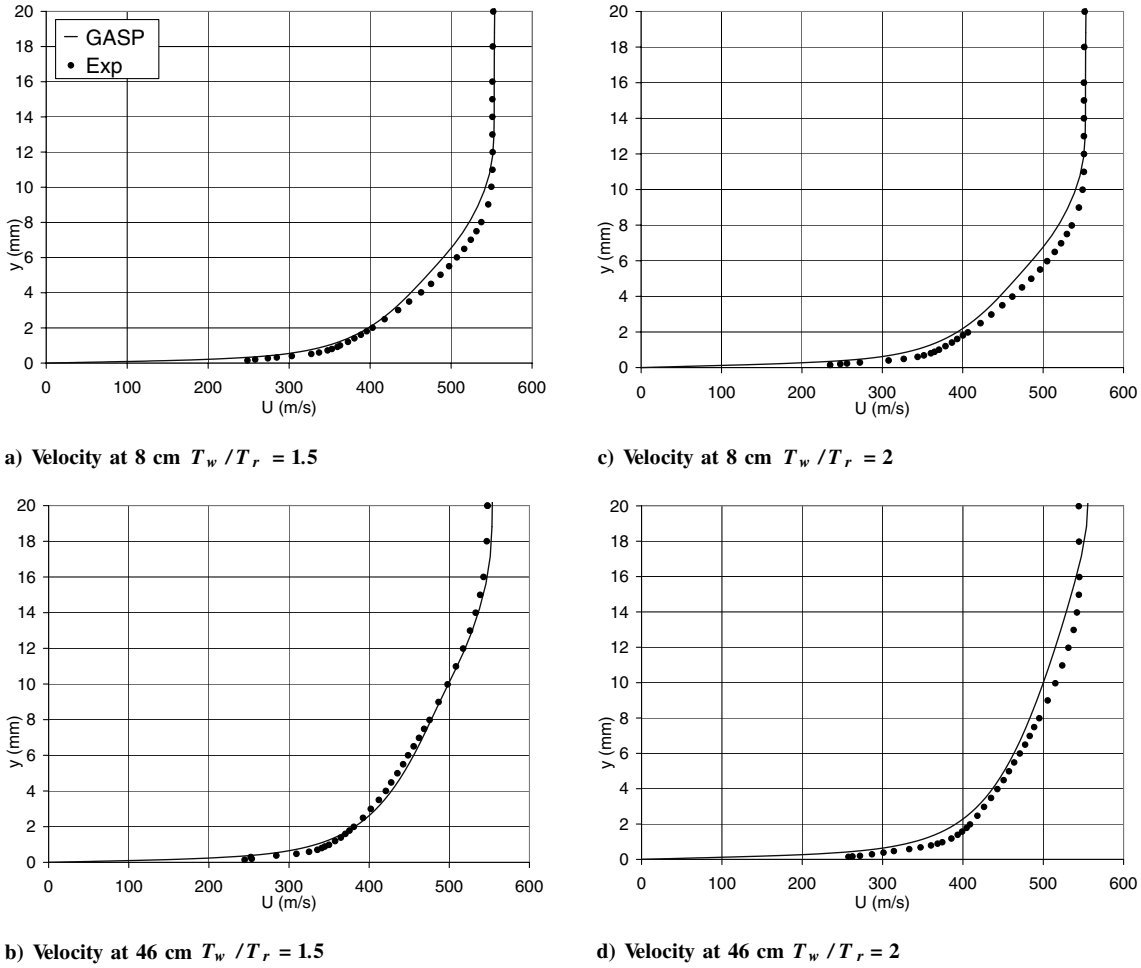

a) Velocity at 8 cm $T_w / T_r = 1.5$

c) Velocity at 8 cm $T_w / T_r = 2$

b) Velocity at 46 cm $T_w / T_r = 1.5$

d) Velocity at 46 cm $T_w / T_r = 2$

Fig. 11 Velocity profiles for supersonic boundary layer with step in wall temperature at $x = 0$ compared with experiment from [3].

cannot be modeled using an algebraic turbulence model (mixing length) or an empirical correlation (N–R correlation). Over-predictions of heat transfer of 20 and 70% are obtained by DeLise and Naraghi [21] for the mixing length turbulence model and the N–R correlation, respectively.

The wall material was not specified by Back et al. [4]. However, the thermal conductivity of the material k_w can be determined from the temperature gradient and the heat flux provided by Back et al. [4].

$$q = k_w \frac{\partial T}{\partial n} \Rightarrow k_w = \frac{q}{\partial T/\partial n} \approx \frac{q\Delta n}{\Delta T} \tag{5}$$

where q is the heat flux and k_w is the thermal conductivity of the wall material. From Fig. 13, k_w is computed by approximating the temperature using the temperature difference between two isotherms separated by a known distance in a region where all the isotherms are parallel to the wall. In that case, the heat conduction is one-dimensional such that the heat flux is constant across the wall. The following value was obtained: $k_w = 27$ W/mK corresponding to AISI 405 stainless steel

The conjugate heat transfer problem is solved by imposing the temperature at the outside wall taken from Fig. 13. The inside wall temperature does not need to be imposed because the boundary condition for conservation of energy at the interface is used as described in Sec. III. The temperature distribution inside the wall, as well as the flowfield, are being determined. The problem was modeled as axisymmetric. The grid containing 6800 cells is depicted in Fig. 14.

As for the previous cases, a grid independent solution was achieved by performing a grid refinement study. Four turbulence models were used, namely, Spalart–Allmaras, Wilcox's 1998 k–ω, Menter's SST, and Chien's k–ϵ. Here, turbulence modeling has an impact on wall temperature (and, therefore, heat transfer rate) as each model reacts differently to the nozzle-favorable pressure gradient which reduces turbulence. The ratio of eddy viscosity to laminar viscosity is shown in Fig. 15. Spalart–Allmaras displays a lower initial amount of eddy viscosity and a fast decrease from the favorable pressure gradient starting upstream of the throat, whereas k–ϵ displays a much higher initial level of eddy viscosity as well as a significant increase near the throat. Spalart–Allmaras offers the best agreement with the experimental data as seen in Fig. 16, in which the computed internal wall temperature is compared with the experimental results. The nozzle Mach number and the nozzle wall temperature contours are depicted in Fig. 17. We notice that the wall temperature distribution (Fig. 17) is similar to the one obtained by Back et al. [4] (Fig. 13).

V. Conclusions

Convective heat transfer simulations have been performed for both subsonic and supersonic flows and compared against experimental data. Predicted Stanton numbers for low Mach number turbulent boundary layers agree with experimental results from Reynolds et al. [1,2] for a constant wall temperature, a step, and a double pulse in wall temperature. Simulations of supersonic boundary layers with a step in wall temperature showed good agreement for velocity and temperature profiles when compared with measurements from Debieve et al. [3], as well as for the skin friction and Stanton number. A methodology used to generate the turbulence information and v-velocity profile based on the work of Zhang and Morishita [23] and Huang et al. [24] was presented. Using this methodology, better agreement was found between experimental and measured velocity and temperature profiles compared with the cases in which the input variables were generated from a flat plate

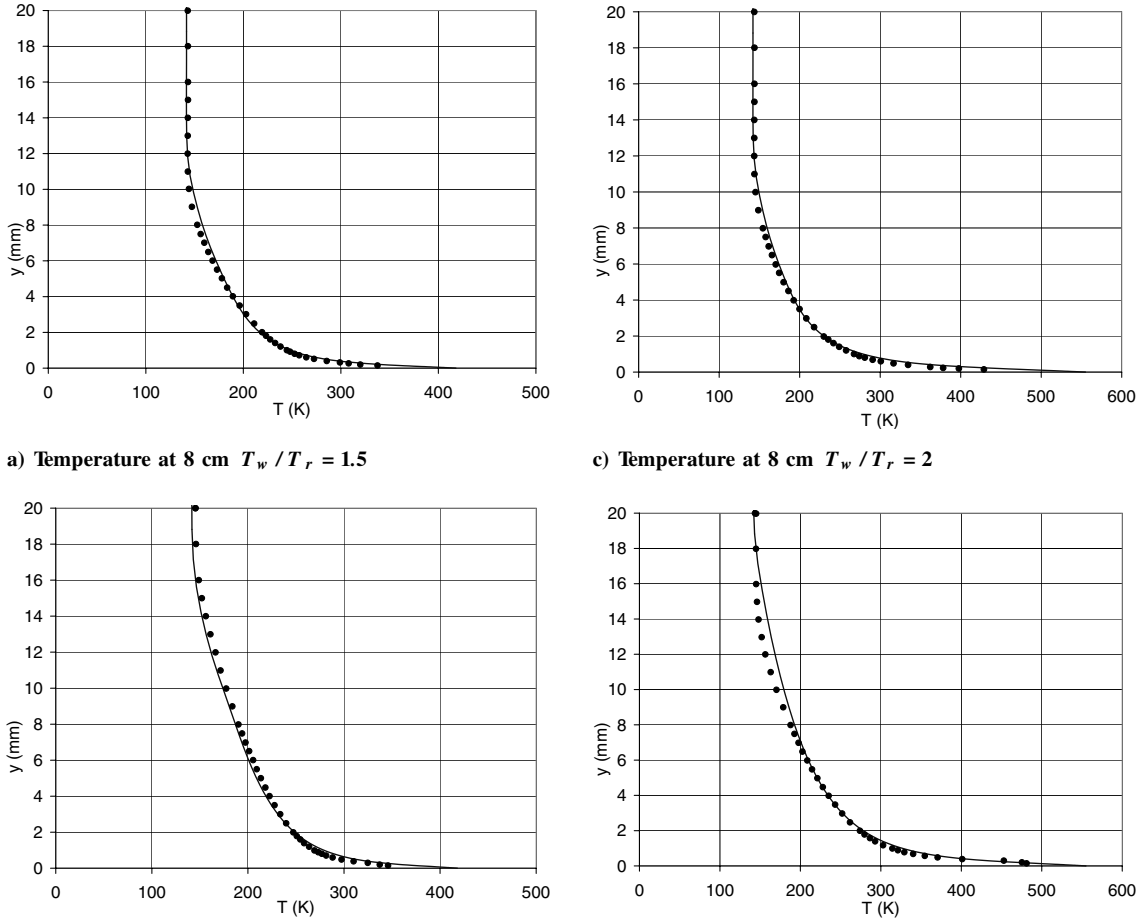

a) Temperature at 8 cm $T_w / T_r = 1.5$

c) Temperature at 8 cm $T_w / T_r = 2$

b) Temperature at 46 cm $T_w / T_r = 1.5$

d) Temperature at 46 cm $T_w / T_r = 2$

Fig. 12 Temperature profiles for supersonic boundary layer with step in wall temperature at $x = 0$ compared with experiment from [3].

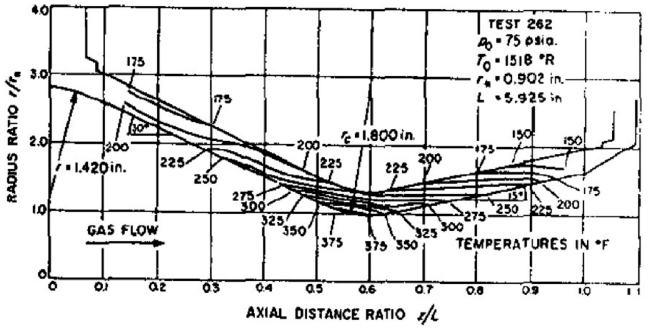

Fig. 13 Temperature distribution inside the nozzle from thermocouple measurements [4] reported by DeLise and Naraghi [21].

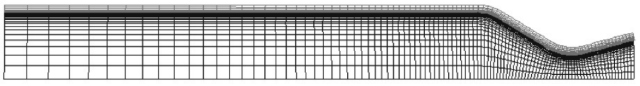

Fig. 14 Cooled nozzle grid containing 6800 cells.

simulation. The algorithm enabling the computation of the temperature and velocity profiles from one integral boundary-layer parameter is particularly useful to generate the inlet velocity profile used for a numerical simulation when limited experimental data are available at that location. This shows the tight interconnection between experimental, analytical, and numerical methods in modeling complex heat transfer problems. Lastly, the flowfield and wall temperature distribution inside a supersonic cooled nozzle is computed using a new CHT algorithm. The temperature distribution along the inside nozzle wall agreed with measurements from Back et al. [4].

Appendix: Generation of Missing Information at the Boundary

When trying to match experimental results using numerical simulations, great care must be taken in accurately reproducing the experimental conditions [23,25]. For the problem, this translates into making sure that the initial boundary-layer profile used for the computation matches that of the experiment. To perform the simulation, the profiles of ρ, u, v, w, p, k, ω must be specified at the inlet. Measurements for all variables are rarely available, therefore, they must be assumed or created. In our case, the temperature and u-velocity profile are available. Assuming constant pressure across the boundary layer, the density profile can be computed from the perfect gas law. The considered flow is two-dimensional such that $w = 0$. This means that the profiles of the v-velocity, turbulent kinetic energy k, and specific dissipation rate ω must be generated. Different approaches were considered.

One approach consists of running a flat plate simulation to the measured integral boundary-layer parameter [25]. This was used for case A. However, for case B, where the incoming boundary layer is developed through a converging–diverging nozzle, the computed and measured u-velocity profiles are dissimilar in the outer region of the boundary layer where adjustment is slower. Another approach consists of using the measured u-velocity profile to compute the turbulence quantities [23]. This was accomplished using the Cebeci–Smith [26] algebraic turbulence model. The approach used is described as follows. For this model, the eddy viscosity is computed differently in the outer and inner layer, such that we have

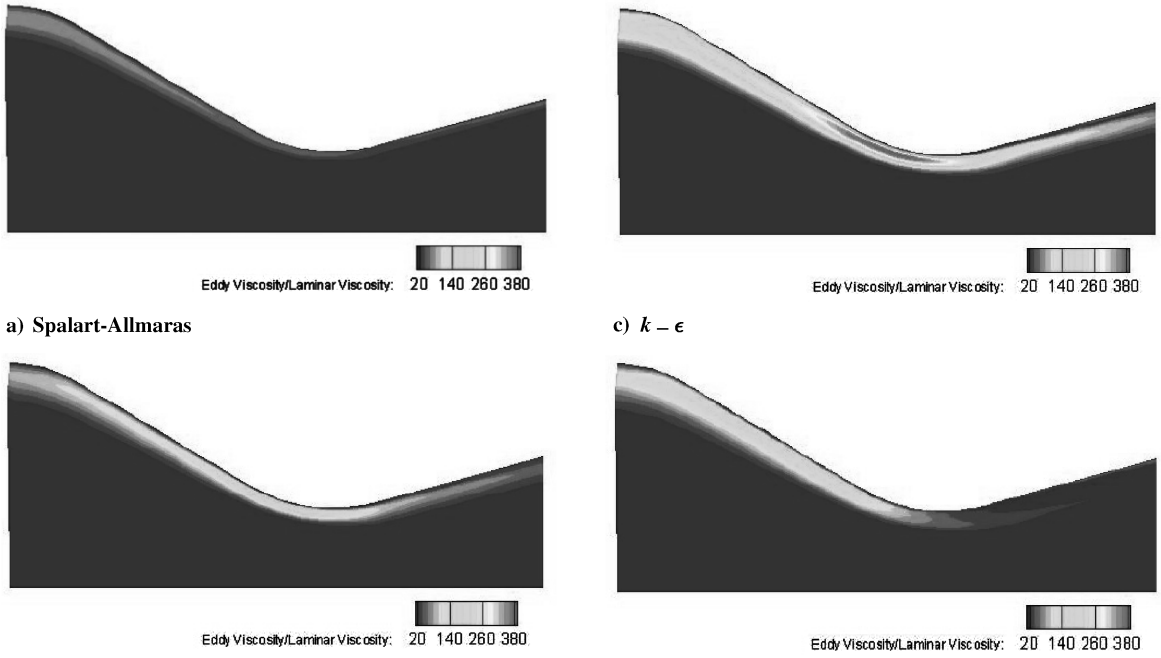

a) Spalart-Allmaras

c) $k-\epsilon$

b) $k-\omega$

d) Menter's SST

Fig. 15 Ratio of eddy to laminar viscosity for a cooled axisymmetric nozzle.

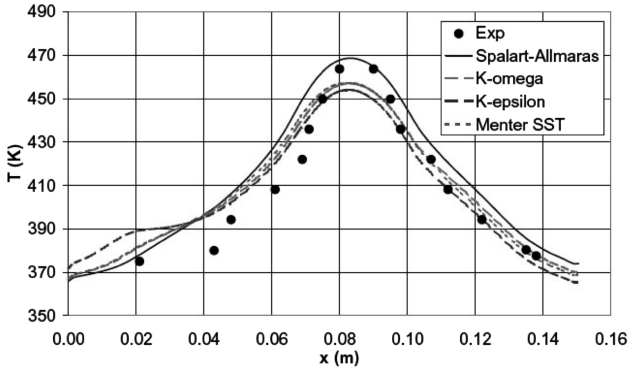

Fig. 16 Inside wall temperature for a cooled axisymmetric nozzle compared with experiment from [14].

$$\mu_t = \begin{cases} \mu_{t_i}, & y \le y_m \\ \mu_{t_o}, & y > y_m \end{cases} \tag{A1}$$

where y_m is the smallest value of y for which $\mu_{t_i} = \mu_{t_o}$. In the inner layer, μ_{t_i} is computed as

$$\mu_{t_i} = \rho l_{\text{mix}}^2 \left[\left(\frac{\partial u}{\partial y} \right)^2 + \left(\frac{\partial v}{\partial x} \right)^2 \right]^{\frac{1}{2}} \approx \rho l_{\text{mix}}^2 \left| \frac{\partial u}{\partial y} \right| \tag{A2}$$

where l_{mix} is the mixing length given as

$$l_{\text{mix}} = \kappa y [1 - e^{-y^+/A^+}] \tag{A3}$$

whereas, in the outer layer we have

$$\mu_{t_o} = \alpha U_e \delta^* F_{\text{kleb}}(y; \delta) \tag{A4}$$

where F_{kleb} is the Klebanoff intermittency function given as

$$F_{\text{kleb}}(y; \delta) = \left[1 + 5.5 \left(\frac{y}{\delta} \right)^6 \right]^{-1} \tag{A5}$$

and δ^* is the boundary-layer displacement thickness

$$\delta^* = \int_0^\delta \left(1 - \frac{\rho u}{\rho_e U_e} \right) \mathrm{d}y \tag{A6}$$

The closure coefficients are

$$\kappa = 0.40, \qquad \alpha = 0.0168, \qquad A^+ = 26 \tag{A7}$$

The principal Reynolds shear stress is computed from the eddy viscosity

$$\tau_{xy} = \mu_t \frac{\partial u}{\partial y} \tag{A8}$$

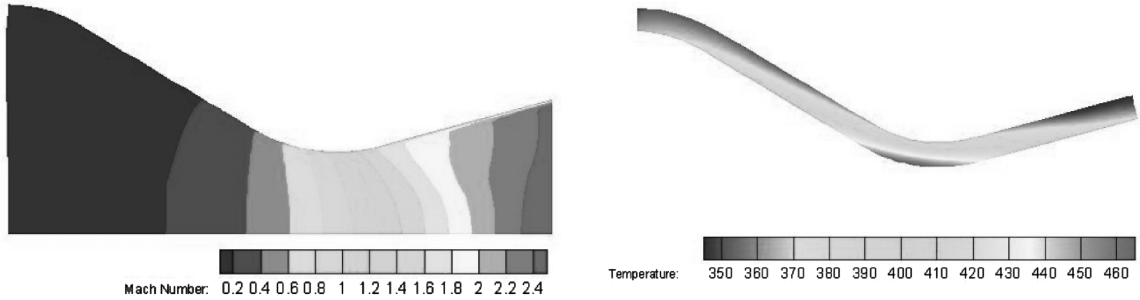

a) Mach number

b) Wall temperature (K)

Fig. 17 Mach number and wall temperature contour for a cooled axisymmetric nozzle using Spalart–Allmaras turbulence model.

Outside the viscous sublayer, the kinetic energy is readily computed using the structural parameter $a = 0.3$

$$\tau_{xy} = ak \Rightarrow k = \frac{\mu_t}{a}\frac{\partial u}{\partial y} \tag{A9}$$

whereas the specific dissipation rate ω is given by

$$\omega = \frac{\rho k}{\mu_t} \tag{A10}$$

Inside the viscous sublayer, we use the asymptotic analysis of the boundary layer performed by Wilcox [8].

$$k = C_2 y^n, \qquad y \to 0 \tag{A11}$$

with $n = 3.23$ and

$$\omega = \frac{C_1 \nu}{\beta^* y}, \qquad y \to 0 \tag{A12}$$

where $\beta^* = 9/100$ is a closure coefficient of the Wilcox k–ω turbulence model and $C_1 = 7.20$. The value of C_2 is found by matching the expression for k valid outside the viscous sublayer [Eq. (A9)] to that valid inside [Eq. (A11)] at the edge of the viscous sublayer located at $y+ = 7$. This yields

$$C_2 = \left(7\frac{\mu_w}{\rho_w u_\tau}\right)^{-n}\left(\frac{\mu_t}{a}\right)\frac{\partial u}{\partial y}\bigg|_{y^+=7} \tag{A13}$$

The methodology used to generate k and ω was validated by employing a flat plate simulation run at the same condition as the experiment from Debieve et al. [3]. The values of k and ω generated from the u-velocity profile (obtained from the flat plate simulation) are compared with those obtained directly from the flat plate simulation.

Figures A1 and A2 show a good agreement so that we are confident in this approach. Next, the v-velocity profile must be generated. An approach based on the work of Zhang and Morishita [23] is used. The missing v-velocity component is found by integrating the Favre-averaged continuity equation

$$\frac{\partial \rho u}{\partial x} + \frac{\partial \rho v}{\partial y} \tag{A14}$$

and because the pressure is constant across the boundary layer, it can be discretized as

$$v_{i,j+1} = \frac{T_{i,j+1}}{T_{i,j}}v_{i,j} - \frac{T_{i,j+1}h_j}{\Delta x}\left[\frac{u_{i+1,j}}{T_{i+1,j}} - \frac{u_{i,j}}{T_{i,j}}\right] \tag{A15}$$

where h_j is grid spacing in the y direction and Δx is the spacing between stations i and $i + 1$. However, to compute v, the u-velocity and temperature profiles must be known at station i and $i + 1$. To generate these two profiles, we use the integral momentum equation:

$$\frac{\mathrm{d}\theta}{\mathrm{d}x} = \frac{C_f}{2} \tag{A16}$$

which, in return, requires knowing the skin friction coefficient and the momentum thickness at station $i + 1$. The following analysis is made to get these quantities. Experimental results and analysis have shown that the compressible boundary layer follows the law of the wall and the law of the wake when the velocity is transformed according to

$$u_c = \int\left(\frac{\rho}{\rho_w}\right)^{\frac{1}{2}}\mathrm{d}u = \int\left(\frac{T_w}{T}\right)^{\frac{1}{2}}\mathrm{d}u \tag{A17}$$

because the pressure is constant across the boundary layer. Starting from the momentum and the energy equation for a two-dimensional boundary layer [27] without pressure gradients, a relation between the temperature and the velocity field can be obtained by

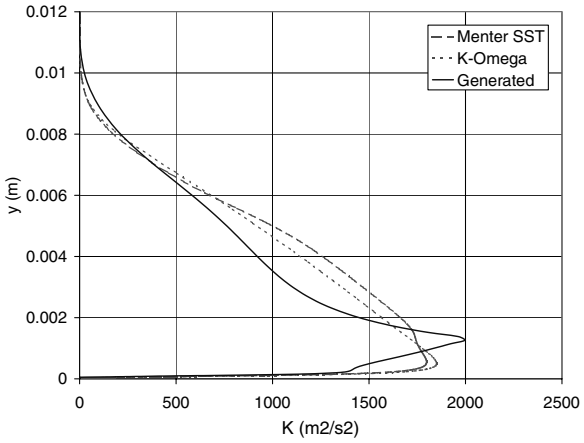

Fig. A1 Generated turbulent kinetic energy compared with computation.

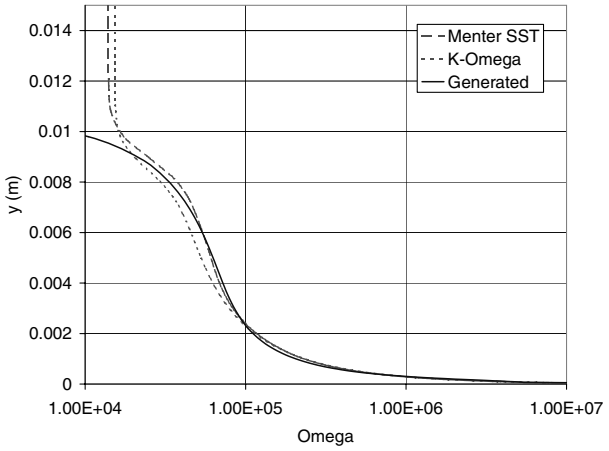

Fig. A2 Generated ω compared with computation.

acknowledging that the convective terms are negligible close to the wall. This simplification enables the integration of the momentum equation which now states that the total stress is constant across the boundary layer

$$(\mu + \mu_t)\frac{\partial u}{\partial y} = \tau_w \tag{A18}$$

This result can be substituted into the energy equation, which is integrated twice, yielding Crocco's integral

$$T = T_w - \frac{Pr_m q_w u}{c_p \tau_w} - \frac{Pr_m u^2}{2c_p} \tag{A19}$$

where the mixed Prandtl number Pr_m, defined as

$$Pr_m = c_p\frac{\mu + \mu_t}{k_f + k_t} \tag{A20}$$

is assumed constant to perform the integration. In practice, for a wall-bounded turbulent flow of air, $Pr_m \approx Pr_t \approx r \approx 0.9$. Using Eq. (A19), Eq. (A17) can be analytically integrated to obtain the Van Driest's transformation

$$u_c = \sqrt{B}\left[\sin^{-1}\left(\frac{A+u}{D}\right) - \sin^{-1}\left(\frac{A}{D}\right)\right] \tag{A21}$$

where

$$A = \frac{q_w}{\tau_w} \tag{A22}$$

$$B = \frac{2c_p T_w}{Pr_t} \tag{A23}$$

$$D = \sqrt{A^2 + B} \tag{A24}$$

The inverse transformation is given by

$$\frac{u}{u_\tau} = \frac{1}{R}\sin\left(\frac{Ru_c}{u_\tau}\right) - H\left[1 - \cos\left(\frac{Ru_c}{u_\tau}\right)\right] \tag{A25}$$

where

$$R = \frac{u_\tau}{\sqrt{B}} \tag{A26}$$

$$H = \frac{A}{u_\tau} \tag{A27}$$

Contrary to Van Driest I transformation [27], the previous is valid for nonunity Pr and Pr_t, as well as nonadiabatic walls because all of these effects are included in Crocco's integral. We use an explicit expression for the law of the wall in the inner region and law of the wake in the outer region which was found by Musker [28]:

$$u_c^+ = 5.424\tan^{-1}\left[\frac{2y^+ - 8.15}{16.7}\right] + \log_{10}\left[\frac{(y^+ + 10.6)^{9.6}}{(y^{+2} - 8.15y^+ + 86)^2}\right] - 3.52 + 2.44\left\{\Pi\left[6\left(\frac{y}{\delta}\right)^2 - 4\left(\frac{y}{\delta}\right)^3\right] + \left(\frac{y}{\delta}\right)^2\left(1 - \frac{y}{\delta}\right)\right\} \tag{A28}$$

where Π is the wake parameter [29] defined as

$$\Pi = 0.55[1 - \exp(-0.24\sqrt{Re_\theta} - 0.298Re_\theta)] \tag{A29}$$

We now have all the analytical expressions required to compute the velocity and temperature profiles from either δ or θ. When θ (or δ) and $[T_w, T_e, U_e, \rho_e, \rho_w, y_i]$ are known, we can compute δ (or θ) and $[u(y_i), T(y_i), C_f, q_w]$ using the following algorithm first developed by Huang et al. [24] and improved by Zhang and Morishita [23].

1) Guess the value of δ (or θ) and u_τ. The estimate $\theta = 7/72\delta$ is reasonable assuming a power law velocity profile with $n = 7$ (see Schetz [27]). An estimation for u_τ can be made from Schoenherr's skin friction correlation [27].
2) Compute q_w using Crocco's integral [Eq. (A19)] evaluated at U_e.
3) Compute u_{c_e} using Van Driest's transformation [Eq. (A21)] evaluated at U_e.
4) Compute $Re_\theta = \rho_e U_e \theta/\mu_w$ and evaluate the wake parameter Π using Eq. (A29).
5) Compute $Re_{\delta_w} = \rho_w u_{c_e}\delta/\mu_w$.
6) Compute $\delta^+ = \rho_w u_\tau \delta/\mu_w$ by solving numerically $Re_{\delta_w} = u_{c_e}^+ \delta^+$ where $u_{c_e}^+$ is obtained from Eq. (A28) evaluated at $y = \delta$.
7) Compute $u_\tau = \delta^+ \mu_w/\rho_w\delta$.
8) Compute $C_f = 2T_e/T_w(u_\tau/U_e)^2$ and $\tau_w = \rho_w u_\tau^2$.
9) Compute u_c^+ at each y_i using Eq. (A28).
10) Compute $u_c = u_c^+ u_\tau$ and u at each y_i from u_c using Van Driest's inverse transformation [Eq. (A28)].
11) Compute T at each y_i from u using Crocco's integral [Eq. (A19)].
12) Compute a new estimate of δ (or θ) from the u-velocity profile using

$$\frac{\theta}{\delta} = \int_0^1 \frac{T_e u}{TU_e}\left(1 - \frac{u}{u_e}\right) \mathrm{d}\eta$$

Steps 2–12 are repeated until convergence. This algorithm was implemented using MATLAB and convergence is reached within less than 10 iterations. For higher Mach numbers, a scaling of y^+ was done by Zhang and Morishita [23]. This was implemented but was not significant for the Mach number considered herein. The following steps are used to compute the v-velocity profile:

1) Compute θ_i from the known temperature and u-velocity profile at station i.
2) Compute θ_{i+1} for known values of θ_i and C_f using the momentum integral equation [Eq. (A16)].
3) From θ_{i+1} compute $u_{i+1,j}$ and $T_{i+1,j}$ using the preceding algorithm.
4) Compute $v_{i+1,j}$ explicitly for the discretized Favre-averaged continuity equation [Eq. (A15)].

The generated v-velocity profile is compared against results from a flat plate simulation in Fig. A3. We notice a difference between the v-velocity profiles among the turbulence models. In the inner layer, the generated v-velocity profile agrees with the one obtained with k–ω, whereas in the outer layer, it reaches the same freestream value as the one obtained using Spalart–Allmaras turbulence model.

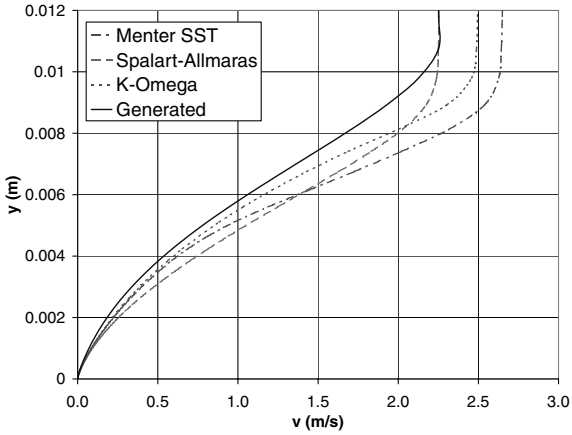

Fig. A3 Generated v-velocity component compared with computation.

Acknowledgment

This work was funded by Arnold Engineering Development Center (AEDC) through the United States Air Force Small Business Innovative Research project under contract FA9101-04-C-0035.

References

[1] Reynolds, W. C., Kays, W., and Kline, S., "Heat Transfer in the Turbulent Incompressible Boundary Layer 1: Constant Wall Temperature," NASA Memorandum 12-1-58W, 1958.
[2] Reynolds, W. C., Kays, W., and Kline, S., "Heat Transfer in the Turbulent Incompressible Boundary 3: Arbitrary Wall Temperature and Heat Flux," NASA Memorandum 12-3-58W, 1958.
[3] Debieve, J., Dupont, P., Smith, D., and Smits, A., "Supersonic Turbulent Boundary Layer Subjected to Step Changes in Wall Temperature," *AIAA Journal*, Vol. 35, No. 1, Jan. 1997.
[4] Back, L., Massier, P., and Gier, H., "Convective Heat Transfer in a Convergent Divergent Nozzle," *International Journal of Heat and Mass Transfer*, Vol. 7, No. 5, 1964, pp. 549–568.
[5] GASP 4.0 User Manual, AeroSoft, 2002, ISBN 09652780-5-0.
[6] Baldwin, B. S., and Lomax, H., "Thin Layer Approximation and Algebraic Model for Separated Turbulent Flows," AIAA Paper 78-257, 1978.
[7] Spalart, P. R., and Allmaras, S. R., "One Equation Turbulence Model for Aerodynamic Flows," *La Recherche Aerospatiale: Bulletin Bimestriel de l'Office National d'etudes et de Recherches Aerospatiales*, Vol. 1, No. 1, 1994, pp. 5–21.
[8] Wilcox, D. C., *Turbulence Modeling for CFD*, 2nd ed., DCW Industries, La Canada, CA, 1998.
[9] Wilcox, D. C., "Reassessment of the Scale-Determining Equation for Advanced Turbulence Models," *AIAA Journal*, Vol. 26, No. 11, 1988, pp. 1299–1310.
[10] Menter, F. R., "Zonal Two Equation k–ω Turbulence Models for Aerodynamic Flows," AIAA Paper 93-2906, July 1993.
[11] Launder, B. E., and Spalding, D. B., "Numerical Computation of Turbulent Flows," *Computer Methods in Applied Mechanics and Engineering*, Vol. 3, No. 2, 1974, pp. 269–289.

[12] Chien, K.-Y., "Predictions of Channel and Boundary-Layer Flows with a Low-Reynolds Number Turbulence Model," *AIAA Journal*, Vol. 20, No. 1, 1982, pp. 33–38.

[13] Lam, C. K. G., and Bremhorst, K., "Modified Form of the k–ϵ Model for Predicting Wall Turbulence," *Journal of Fluids Engineering*, Vol. 103, No. 3, 1981, pp. 456–460.

[14] Neel, R. E., Godfrey, A. G., and Slack, D. C., "Turbulence Model Validation in GASP Version 4," *33rd AIAA Fluid Dynamics Conference and Exhibit*, AIAA Paper 2003-3740, 2003.

[15] Nagano, Y., *Closure Strategies for Turbulent and Transitional Flows*, Modelling Heat Transfer in Near-Wall Flows, Cambridge Univ. Press, Cambridge, England, UK., 2002, Chap. 6, pp. 188–247.

[16] Kays, W., Crawford, M., and Weigand, B., *Convective Heat and Mass Transfer Fourth Edition*, McGraw–Hill, New York, 2005.

[17] Brinckman, K., Kenzakowski, D., and Dash, S., "Progress in Practical Scalar Fluctuation Modeling for High-Speed Aeropropulsive Flows," *AIAA 43rd Aerospace Sciences Meeting*, AIAA Paper 2006-8037, 2006.

[18] Sommer, T., So, R., and Zhang, H. S., "Near-Wall Variable-Prandtl-Number Turbulence Model for Compressible Flows," *AIAA Journal*, Vol. 31, No. 1, Jan. 1993.

[19] Bradshaw, P., *Topics in Applied Physics, Volume 12: Turbulence*, 2nd ed., Vol. 12, Springer–Verlag, New York, 1978.

[20] Roe, P. L., "Approximate Riemann Solvers, Parameter Vectors, and Difference Schemes," *Journal of Computational Physics*, Vol. 43, No. 2, 1981, pp. 357–372.

[21] DeLise, J., and Naraghi, M., "Comparative Studies of Convective Heat Transfer Models for Rocket Engines," *31st AIAA/ASME Joint Propulsion Conference and Exhibit*, AIAA Paper 1195-2499, 1995.

[22] Liu, Q., Luke, E., Cinnella, P., and Tang, L., "Coupling Heat Transfer and Fluid Flow Solvers for Multi-Disciplinary Simulations," *AIAA 42nd Aerospace Sciences Meeting, Reno, NV, 5–8 Jan. 2004*.

[23] Zhang, J., and Morishita, E., "Efficient and Accurate Way of Posing Inflow Profile Boundary Conditions," *Transactions of the Japan Society for Aeronautical and Space Sciences*, Vol. 15, Aug. 2004, p. 80.

[24] Huang, P., Bradshaw, P., and Coakley, T., "Skin Friction and Velocity Profile Family for Compressible Turbulent Boundary Layers," *AIAA Journal*, Vol. 31, No. 9, Sept. 1993.

[25] Wong, W., and Qin, N., "Numerical Study of Transonic Flow in a Wind Tunnel Over 3D Bumps," *AIAA 43rd Aerospace Sciences Meeting*, AIAA Paper 2005-1057, 2005.

[26] Smith, A., and Cebeci, T., "Solution of the Boundary-Layer Equations for Incompressible Turbulent Flow," *Proceedings of the 1968 Heat Transfer and Fluid Mechanics Institute*, Stanford Univ. Press, Stanford, CA, 1968, pp. 171–191.

[27] Schetz, J., *Boundary Layer Analysis*, Prentice–Hall, Upper Saddle River, NJ, 1993.

[28] Musker, A., "Explicit Expression for the Smooth Wall Velocity Distribution in a Turbulent Boundary Layer," *AIAA Journal*, Vol. 17, No. 6, June 1979.

[29] Cebeci, T., and Smith, A., *Analysis of Turbulent Boundary Layers*, Academic Press, New York, 1974.